https://doi.org/10.3311/PPci.37713

Periodica Polytechnica Civil Engineering

Failure Mechanism of the Toppling Rock Slope with Different Numbers of Free Faces Caused by Excavation: a Case Study in Jiacha Hydropower Station (China)

Shao-Ping Huang[1,2], Kai-Ming Cao[1,2], Chang Zhou[3], Heng-Lin Xiao[1,2], E-Chuan Yan[4*], Lu Cong[5]

[1] Key Laboratory of Health Intelligent Perception and Ecological Restoration of River and Lake, Ministry of Education, Hubei University of Technology, no. 28, South Lee Road, 430068 Wuhan, Hubei Hongshan, China
[2] School of Civil, Architectural & Environmental Engineering, Hubei University of Technology, no. 28, South Lee Road, 430068 Wuhan, Hubei Hongshan, China
[3] School of Resources and Geosciences, China University of Mining and Technology, no 1, Daxue Road, Quanshan District, Xuzhou, 221116 Jiangsu, P.R. China
[4] School of Engineering, China University of Geosciences, no. 388, Lumo Road, 430074 Wuhan, Hubei, Hongshan, China
[5] College of Electrical and Power Architecture, Shanxi University, no. 79 West Street Yingze, 237016 Taiyuan, Shanxi, China
[*] Corresponding author, e-mail: yyc1969china@outlook.com

Received: 18 June 2024, Accepted: 07 August 2024, Published online: 30 August 2024

Abstract

Toppling failure is a widespread failure mode in natural and excavated rock slopes and threatens the construction and operation of important infrastructure, such as hydropower and transportation corridors in southwest China. Therefore, comprehending the mechanisms underlying toppling is essential for predicting and preventing relevant landslides. In this study, external deformation monitoring equipment, multipoint deep displacement meter and data acquisition equipment were conducted on the study area to explore the failure model and deformation characteristic of the toppling rock slope with different numbers of free faces. The field monitoring results suggested that the groundwater and unloading effect caused by excavation initiated this slope with one free face, which subsequently deformed gradually at a constant velocity. Thereafter, the displacement vectors progressed toward the free face, and the rock layers gradually slanted downslope. After the slope failed, it was separated into two sections with double and three free faces, respectively. The failure models of these two sections were analyzed numerically, and the results show that the deformation of the double free faces rock slope is primarily caused by wedge sliding along the intersection line of two discontinuities; the three free faces rock mass slope may bend first and then slide along a discontinuity. The study deepens the understanding of toppling rock slopes and provides a theoretical framework for anticipating and avoiding the deformation trends of such slopes.

Keywords

toppling rock slope, free faces, failure mechanism, on-site monitoring, numerical simulation

1 Introduction

Toppling rock slope is defined as a slope in which the strike of the rock strata and the strike of the slope face are nearly parallel or intersect at a small angle, and the rock strata tend to be opposite to the slope [1–5]. It is a typical rock slope and widely distributed in the large hydropower slope, highway slope, open-pit mining slope, and other engineering fields [6–10]. The failure of the toppling rock slope has the characteristics of large scale, suddenness, and threat, such as Frank landslide (Canada), Brilliant landslide (USA), Ghurgar rockfall (Beru), Yanchihe rockfall, and Jinchuan slope (China) [11]. Those toppling rock slopes caused huge economic losses and casualties, and thus it is important to analyze the deformation characteristics of this type of slope [12–14].

This type of slope is prone to toppling and deformation mainly due to the influence of initial stress, rock property, and slope structure [15–20]. The deformation of the toppling rock slope directly affects the geological structure. Therefore, it is important to study the failure mechanism and deformation characteristics of toppling rock slope. Some achievements have been made in the study of toppling rock slope. The concept of toppling was first proposed [21]. Subsequently, Goodman and Bray [22] categorized toppling

Cite this article as: Huang, S.-P., Cao, K.-M., Zhou, C., Xiao, H.-L., Yan, E.-C., Cong, L. "Failure Mechanism of the Toppling Rock Slope with Different Numbers of Free Faces Caused by Excavation: a Case Study in Jiacha Hydropower Station (China)", Periodica Polytechnica Civil Engineering, 2024. https://doi.org/10.3311/PPci.37713

failure into three types: block toppling, flexural toppling, and block-flexural toppling, and presented a simplified stability calculation formula for block toppling failure. After that, some researchers systematically studied the deformation, failure laws, and failure mechanism of the toppling rock slope, denoting that various factor, such as the dip, slope angle, and rock structure, control the failure type and the scale of the toppling rock slope [23–25]. Han and Wang [12] extensively studied the toppling mechanism, identifying several influencing factors, and determined that toppling structural planes significantly restrict slope deformation. Bobet [26] computed the conditions of block toppling and sliding using the mechanics theory, assuming the rocky slope as a continuous medium. Yan et al. [2] proposed that the geometric feature parameters (slope angle, strata dip, rock flexibility) of the toppling rock slope have the most significant influence on its toppling deformation. Yokoyama [27] found through detailed geological and geomorphological analysis that deep gravity deformation causes slate bending and toppling on slopes. In order to study the toppling slope failure mechanism during excavation, Zhu et al. [9] modeled excavation and delineated four toppling failure stages: initial compression, fracture creation, crack propagation, and sliding surface formation. During this process, many researchers performed systematic investigations of the toppling behavior of rock slopes to explore the failure mechanism and to develop the toppling failure model [14, 28–32].

After decades of efforts, rich results have been achieved in the research of toppling rock slopes. However, much of current research mainly focuses on revealing the deformation characteristics and failure mechanism of the toppling rock slope with one free face [33–37]. Only a few scholars have studied the deformation and failure characteristics of the toppling rock slope under the conditions of two free frees [38–40]. In the realm of engineering, rock slopes, particularly those prone to toppling, represent complex spatial geometrical bodies that may exhibit multiple free faces under excavation conditions. The current body of research has yet to fully explore the deformation characteristics and failure mechanisms of toppling rock slopes with varying numbers of free faces. Addressing this significant research gap not only holds the potential to advance our fundamental understanding of geotechnical engineering but also carries wide-ranging implications for safety and efficiency in construction and excavation practices. By investigating these aspects, we can propose optimal excavation strategies and preventive measures, thereby contributing to safer and more effective slope stabilization efforts.

With the construction of hydropower projects in southwest China, numerous large-scale toppling failures have been exposed along the Yarlung Zangbo River [41]. Predominantly, the lithology of the slope in this area primarily consists of interbedded sandstone and slate, leading to a frequently observed toppling mode caused by the excavation due to engineering construction. Therefore, it is of practical significance to study this failure mechanism of the toppling rock slope with different free face conditions. The objective of this study was to obtain the failure mechanism and deformation characteristic of the toppling rock slope with different numbers of free faces. The slopes downstream of the dam foundation on the right bank of the Jiacha hydropower on the Yarlung Zangbo River are taken as research objects. Field information, including inclinometer readings, crack investigation and surface and deep monitoring, is obtained from the external deformation monitoring equipment, multipoint deep displacement meter and long-term observation on site. At the same time the numerical simulation model was constructed based on field observation data. This model simulates the deformation characteristics of rock slopes composed of toppling rock slope under varying free face conditions, and concludes the failure mechanism based on the simulation results.

2 Geography and geomorphological setting

2.1 Regional settings

The Jiacha hydropower station is located on the Yarlung Zangbo River, in Xizang Province, China (Fig. 1(a)). It is located in the eastern part of the globally renowned latitudinal tectonic zone, namely the Tethys Orogenic Belt. It belongs to the primary structure. The Yarlung Tsangpo Fault Zone, a first-order structural feature, diagonally crosses the Yarlung Tsangpo River approximately 3 km downstream of the dam site. It generally follows the course of the Yarlung Tsangpo River, trending nearly east-west, with a steep inclination towards the south or north, forming a slightly southward convex arc, spanning over 1000 kilometers. This fault zone represents a massive tectonic boundary in the southern part of the Qinghai-Tibet Plateau, resulting from the tectonic evolution of the Indian Plate subduction and collision with the Eurasian continent. Along this fault zone, there are development of Cretaceous ophiolite suites, mixed rock zones, and Mesozoic-Cenozoic mafic and ultramafic intrusive rocks. Furthermore, it controls the distribution of early Mesozoic acidic and alkaline intrusive rocks as well as lava eruptions on the northern side. Since the Himalaya movement, the whole Yarlung Zangbo River has been involved

in a totally new tectonic movement period, which mainly consists of intermittent uplift, tilt and slow sedimentation. Meanwhile, under the action of intensive fluvial incision, the present high-steep natural slopes are eventually formed.

2.2 Study site

The Jiacha hydropower station creates a reservoir of 2.66×10^7 m^3 with an average height of 87 m. The operating water level is 3246 m. The installed capacity of the station is 360 MW. The segment of the river flows in the direction of N50°E, with a "U"-shaped wide valley. The right bank retains a residual II-grade terrace. The width of the river is approximately 20–30 m, and the elevation of the terrace ranges from 3255 m to 3256 m. The lower part of the terrace consists of steep bedrock slopes.

The study area is described as an unstable mountainside, which is above 700 m high. It is situated on the left bank of the Yarlung Zangbo River and is far away from the hydropower station about 230 m. It is distributed at elevations ranging from 3200 m to 3310 m, with a height of about 110 m. The planar shape of the slope is trapezoidal (Fig. 1(b)), and its' slope gradient is from 35° to 40° (Fig. 1(c)). The overall terrain shows that it is lower in northern regions than that in southern regions. The lithology of the slope rock mass is mainly composed of the interbedded structure of thin-medium thick layer rock mass, which is mainly carbonaceous slate with sericite quartz schist (T_3j^1). A fault belt (EW/S70°) with a length of about 630 m is developed in the upper part of the rock slope, and the width of the fault fracture zone is about 1 m–3 m. In addition, three sets of major control structural planes have been identified through field investigations: 1) the occurrence of the first dominant joint surface is EW/S50°–70° which intersects with bank slope at a small angle; 2) the second one is SN/W80°–85° with a space of 0.1–0.3 m, which is perpendicular the strata; 3) the third one is N50°60°W/NE40°–45° with a space of 0.3–1.0 m and intersects with the bank slope at a small angle. The slope was excavated with aims to create the diversion canal (Fig. 1(d)), resulting in the formation of many unloading cracks. The loosened fractured zone extends to a depth of about 1 m at the road.

3 Deformation characteristics of the topping rock slope

Several cracks were found mainly near the No. 2 highway and on the platform at the elevations of 3255 m and 3240 m after the heavy snow on January 21, 2015. To study the deformation characteristics of this rock slope and landslide monitoring and warning, a real-time monitoring system, including surface monitoring and deep displacement monitoring,

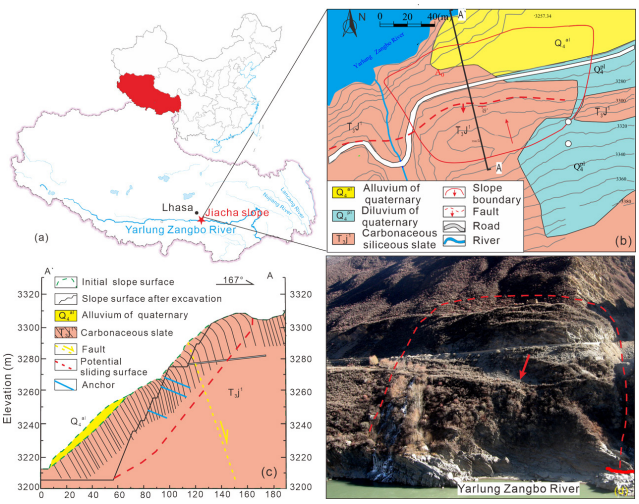

Fig. 1 a) The Location of the Jiacha slope; b) Topographic and structural outline map; c) Cross-section profile of the slope; d) Panoramic view of Jiacha slope before excavation

was equipped to record the deformation characteristics of the slope (Fig. 2). Eighteen temporary monitoring points (D1–D18) were installed on the surfaces of the slope. The spacing of the monitoring points is about 26 m along the sliding direction. Four multi-point extensometers were installed on the upslope. One extensometer contains five measurement units with a vertical spacing of 10 m, 15 m, 20 m, and 25 m from the shallow part of the slope to the inside.

3.1 Deformation of the toppling rock slope

According to the deformation characteristics based on the monitoring results, and failure mechanism, this slope was divided into four parts (Fig. 3): the bending deformation areas (A1, A2, A3), the collapse areas (A4, A5, A6), the potential collapse areas (B and C) and the slope influence area (D). Their deformation characteristics were analyzed in detail.

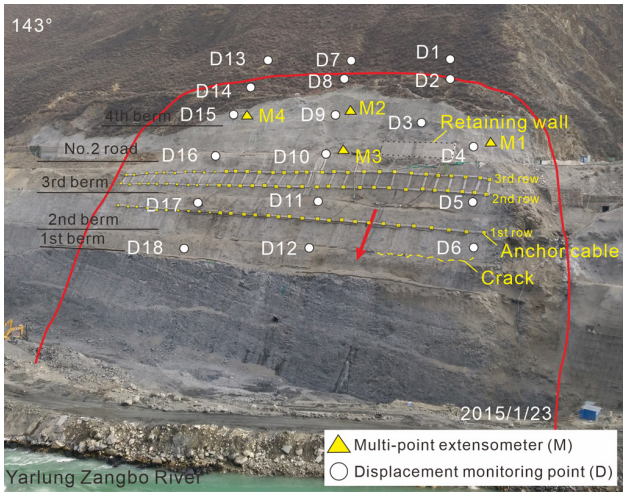

Fig. 2 Monitoring system of the toppling soft rock slope

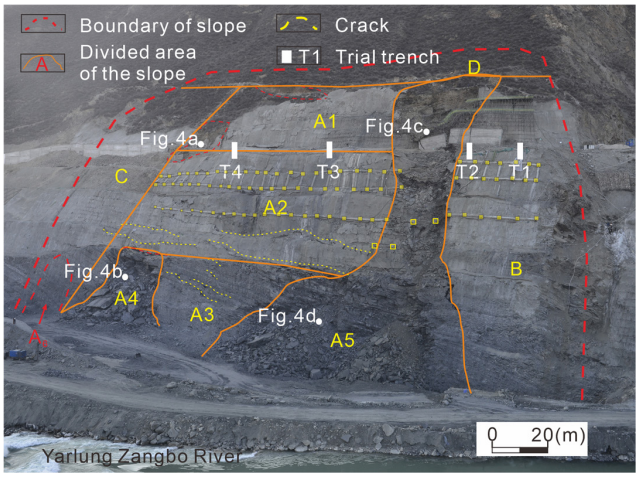

Fig. 3 Division of deformation area. (Note the white rectangles are the location of four trial trenches named T1 to T4.)

Collapse area: A4 and A5 were firstly collapsed and deposits accumulated at the toe of the slope. The shapes of those areas were a pyramid with approximately 500 m^2 and 3300 m^2, respectively. There were some cracks on both sides of the A4 and A5. The majority of the deposit are debris (Fig. 4(b, d)).

Bending deformation area: this area is divided into three parts based on their deformation characteristics: fracture zone (A1), bulging zone (A2), and dilatancy zone (A3). (1) Fracture zone A1 is located on the upstream side of the slope and some tension cracks developed with a length of 2–3 m (Fig. 4(c)). The scarps were formed at the rear part of the A1 area. A steep scarp with a height of 5–10 m is formed locally (Fig. 4(a)). The deformation and failure of the rock mass were severely dumping, bending, and breaking, and its structure had been damaged, with the majority of it scattered. (2) Bulging zone A2 elevation is between 3233 m to 3274 m. This part was compressed by the A1 area and gradually deformed. (3) Dilatancy zone A3 elevation is between 3203 m to 3233 m. The deformation of the A3 area was mainly fracturing dilatancy, and its' damage depth was obviously reduced. Under the effect of the A4 and A5 area, there are multiple sets of tensile cracks parallel to the slope at the head of the A3 area, the vertical displacement of cracks ranges from 0.1–0.3 m. The slope tends to bending toppling deformation.

Potential sliding area (B and C area): B and C area are located on both sides of the slope and are currently stable as a whole, with only partial cracks developing on the slope surface, but under the combined effect of groundwater and unloading, further deformation and damage to the slope will occur, leading to overall instability. For example, the toe of the C area (A6) collapsed on Feb. 9, 2015 (Fig. 3), and many cracks were formed.

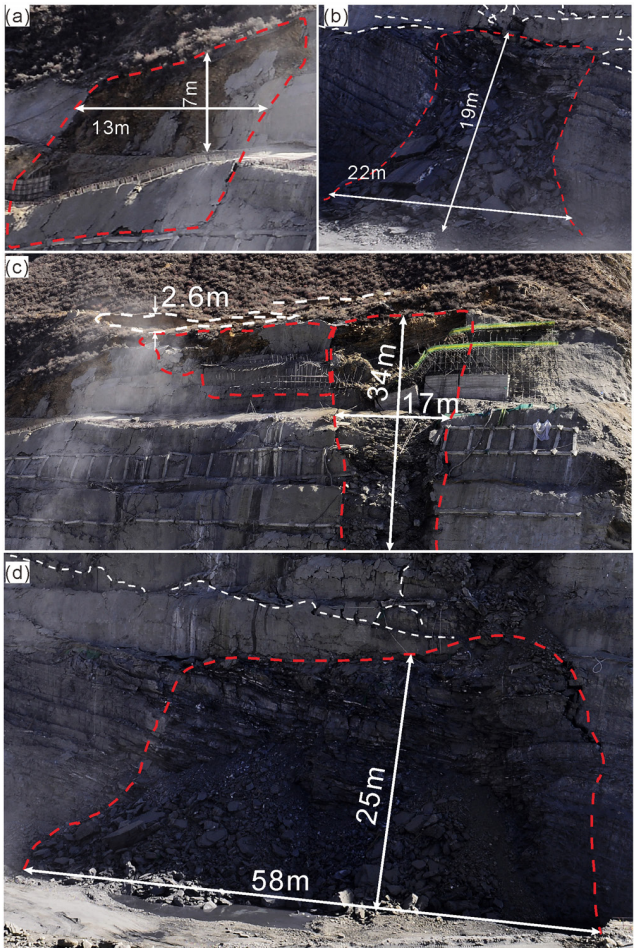

Fig. 4 Deformation characteristics of sub-divided landslide. a) collapse in the lower left corner of the A1 area; b) A4 area; c) A1, D, and upper part of A5; d) downhill portion of the A5 area

Some cracks were found at the toe of the second berm on 23 Jan 2015 (Fig. 2). The field investigation found that the deformation of the slope accelerated after the blasting on 28 Jan 2015. Many cracks were mainly generated in the middle and uphill part of the slope. On 1 Feb 2015, there was some rockfall on the downhill of the slope surface, and the uphill part of the A5 failed. At 8:46 a.m., the A4 and the downhill of the A5 area rapidly collapsed and accumulated at the toe of the slope. At 7:30, 4 Feb 2015, the rapid collapse of the rock mass behind the A5 area had led to the formation of two free faces at this collapse site, and the No. 2 road and anchor cable system failed. Consequently, the collapse broke in the front part of the slope, and the rock mass was flaky. Many tensional cracks developed on the slope surface, and some cracks ran through the slope. Furthermore, some shear cracks were found during this process.

Field investigation and the excavation of the trial trench found that the mainly strata unit is the gray flaggy carbonaceous slate, which is a typical rock mass with a broken

structure. It should be noted that the trial trench explored that the inclination of the strata gradually decreased from upstream to downstream. In the T1 trial trench, the inclination of the strata in the stable zone (0–3 m) is 70° (Fig. 5(a)), but in the deformation zone, it changes to 45° (Fig. 5(b)). A crack was observed with the width of 5–10 mm (Fig. 5(b)), and other one also was found in the rock perpendicular to the strata. In the T2 trial trench (Fig. 6(a)), the inclination decreased from 55° to 10° from the uphill to the downhill side of the trial trench. Three cracks were formed perpendicular to the sliding direction of the slope and extended into the slope (Fig. 6(b)).

3.2 Results of the surface displacement monitoring of the slope

Fig. 7 shows the accumulated displacement of the slope surface. All the curves have a similar trend: the displacement of the measurement points increased with a constant velocity initially and then rapidly accelerated after Feb 2. The D2 and D3 had the largest displacement in the potential sliding area (Fig. 7(a)). Furthermore, they gradually increased at an average velocity of 13 mm/day, but their velocity rapidly increased to 80 mm/day after Feb 3. The displacement of the middle portion (D4, D5, and D6) is smaller than that of D2 and D3 whose locations are close to the collapse area. However, the displacements at points D1, D7, and D13 were very small (< 5 mm) (Fig. 7(b)). In addition to the above points, other monitoring points were located in the bending deformation area. The displacement of the rock slope

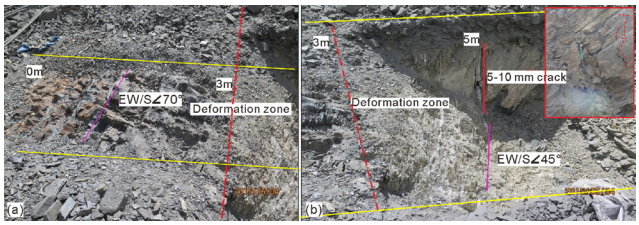

Fig. 5 Strata exposed by T1 trial trench, a) upstream of the B area, b) downstream of the B area

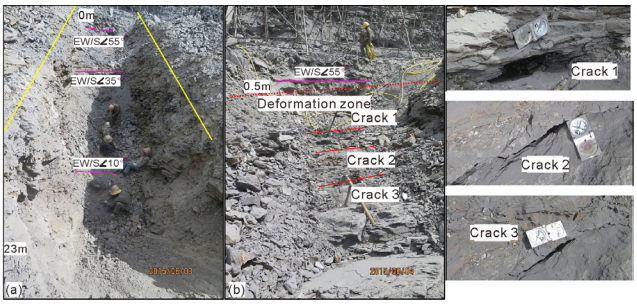

Fig. 6 Strata exposed by T2 trial trench, a) upstream of the B area, b) downstream of the B area

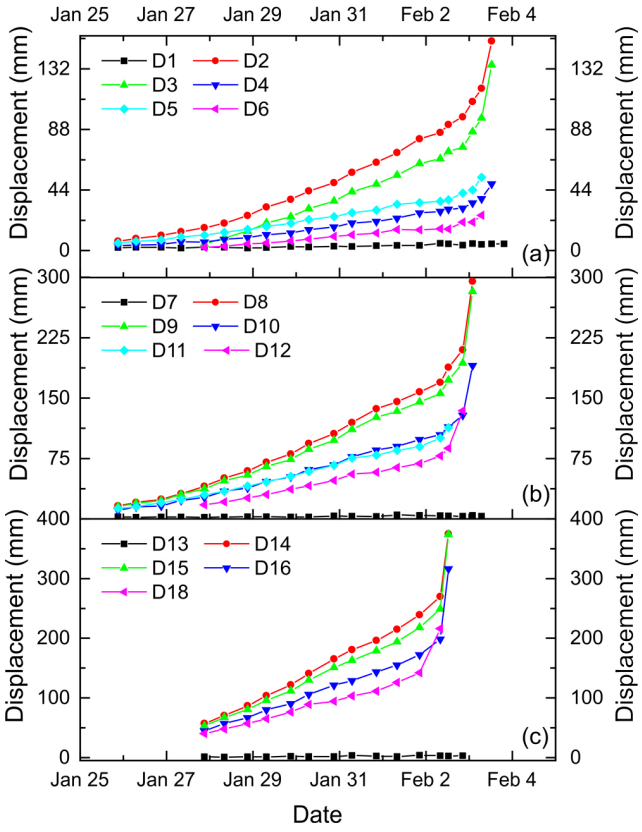

Fig. 7 Relation curves of the long-term external deformation monitoring data with time, a) B area, b) A area, c) C area

gradually decreased from the upstream to downstream and from the east side to the west side. The displacement of those points tended to rapidly increase with a high velocity. For example, the average rate of the D14 (Fig. 7(c)) was 38 mm/day which is three times of the D2.

The 3D displacement vectors of the monitoring points are depicted in Fig. 8 at different times. All monitoring points have different degrees of deformation in B area. This is a significant finding with regards to no matter in which direction, D1 displacement was the smallest, while D2 was the largest. In other words, the displacement of two adjacent points had a significant difference in each direction. From the top to bottom of the monitoring points except for D1, the displacement gradually decreases, which indicates that the anchoring project on-site limits the development of slope cracks. Furthermore, Fig. 8 shows that all monitoring points in B area had the largest displacement in the X direction. However, the collapse of the downhill part of the slope provided a free face for the B area. As a result, a slope with three free faces was generated, this slope occurred a typical 'nodding and slouching type' toppling deformation due to gravity and external forces. The slope slipped along the sliding direction and the deformation mainly occurred in the middle

portion. As shown in Fig. 8, the different portions have different sliding directions. The displacement vectors direction of the A1 area firstly vertically downward, and then gradually changed to the horizontal direction. At the same time, the amount of the vectors also increased. However, in the A2 area, the direction of those vectors became more and more horizontal. The horizontal angle of the displacement vectors at the uphill side of the A2 (D12, D18) gradually decreased and their amount also decreased. In the B area, the displacement vectors' direction and values were different from that in the A1 and A2. First, the directions of the vectors slope downward (Fig. 8(a)), but on February 2, they become upwards slope (Fig. 8(b)). Secondly, the values of the vectors were smaller than other monitoring points. Compared with the monitoring results of the A1, A2 and C areas, it is clear that the total deformation, the displacements of X, Y and Z direction were produced at the same elevation in the A1 and A2 areas are obviously greater. After the deformation and damage of the slope between the A1, A2 areas and B profile, the slope on both sides were provided with a proximal surface. A1, A2 areas and the C area are located form two faces, resulting in ‚book dumping' of the slope, which can explain that the displacement of A1 and A2 areas is larger than that of the C area. According to the detailed field investigation with the borehole survey, it is known that the depth of burial of the damaged surface is greater at the location close to the side hollow surface.

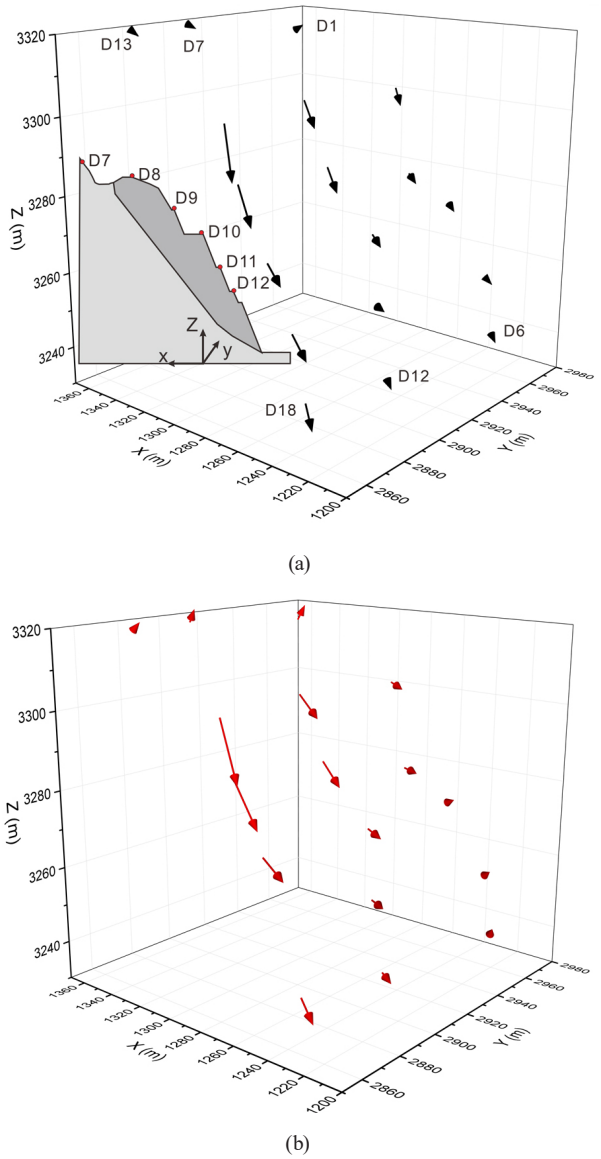

Fig. 8 3D displacement velocity of the monitoring points on (a) Jan 30; (b) Feb 2

3.3 Results of the deep displacement monitoring of the slope

In order to understand the inside deformation characteristics of the slope, multi-point extensometers were installed at 0 m, 10 m, 25 m, 45 m and 65 m away from the slope surface. The monitoring results are as graphically demonstrated in Fig. 9. Firstly, the monitoring points at M2 (Fig. 9(b)), which

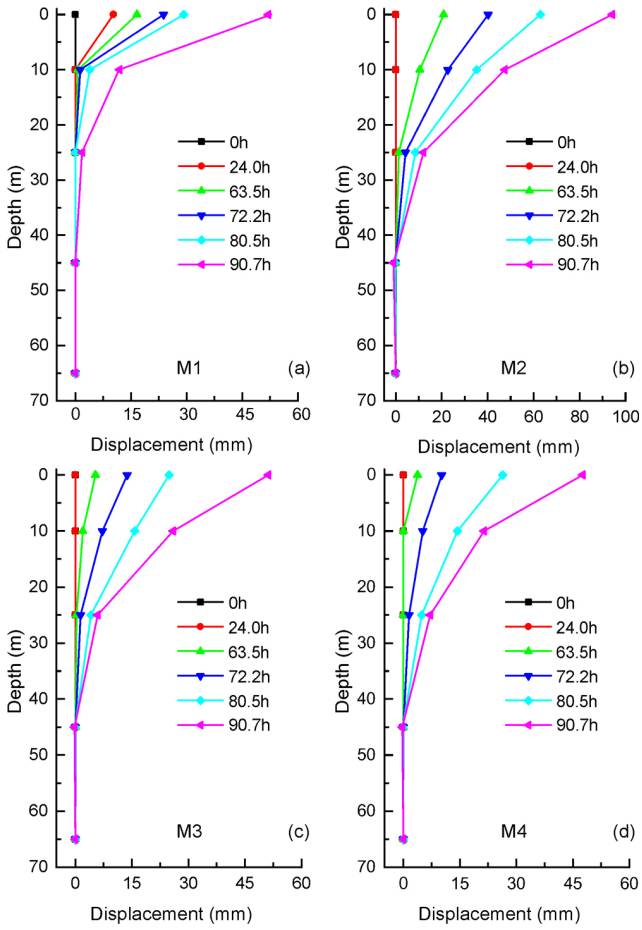

Fig. 9 Multipoint monitoring results, a) M1, b) M2, c) M3, D) M4

is close to the collapse zone A1 with two free faces, had the largest displacement and deformation depth compared with others. The deformation of these monitoring points gradually decreased as the increase of depths and reach 0 mm at depths of 25–35 m, which indicated that the deformation depth of the slope is 25–35 m. The monitoring point at M3 (Fig. 9(c)) had a lower evaluation and smaller displacement than M2. Secondly, the displacements of the monitoring points accelerated, especially near the shallow slope. As result, the collapse area was produced. Moreover, it can be seen from Fig. 9 that at the beginning of the monitoring work, there is no displacement at all points at the time of 0 h, but at 24 h, the deformation first begins at M1 and reaches a depth of 10 mm. After that the deformation rate begins to decrease gradually at M1 after the collapse area occurred and is mainly attributed to the fact the anchoring system still had a reinforcement effect to stabilize the slope. Thirdly, it also can be seen that the maximum displacement of M2 reached 85 mm which is larger than that of M3 (44 mm), indicating that the rear of the slope squeezes the front movement. In addition, the displacement monitoring results (Fig. 9 (a, b, c, d)) also show that the displacement gradually decreased from upstream to downstream, indicating the deformation model of the slope is toppling deformation. A5 area failure provides a new free face for B area and a new rock slope with three faces is generated. The shallow part of the slope integrally slips along the sliding surface. However, in the deformation area, the monitoring points are closer to the deposit area (A5) and have larger displacement, which could be inferred that the slope gradually deformed towards two open surfaces. The results of the drilling and deep deformation monitoring also show that the closer to the free face, the greater the depth of the deformation zone. This can be explained by the fact that the formation of the upstream collapse area gives rise to one free face turned into two free faces in the slope. In addition, this agrees well with the external deformation monitoring results.

4 Method of numerical simulation and results

Free face geometry shape has a significant effect on the deformation characteristics and failure mechanism of the rock slope [34]. Jiacha slope first had one free face, and then local collapse occurred which divided the slope into two slopes with double, and three free faces, respectively. In order to further explore the deformation and failure characteristics, deformation evolution process and genetic mechanism of the toppling rock slope with different numbers of free faces. The three-dimensional geological generalized model of the slop is constructed by 3DEC, and the deformation and failure modes of the toppling rock slope under different free-face numbers are analyzed in the process of slope deformation and evolution. At the same time, the stability of the Jiacha slope after the local sliding mass failed was analyzed numerally to evaluate the influence of the free-face number on the slope deformation. Therefore, the collapse area is excavated through the 3DEC command flow to establish a simplified geometric model of the slope as shown in Fig. 10. And according to the geological conditions of the site the joint model was applied to simulate the stratification, joints, and faults in the model.

4.1 Basic computation conditions and parameter selection

In the numerical simulation, the joint contact surface adopts the Coulomb sliding model, where the shear dilation angle in the Coulomb sliding displacement model is a linear function within the shear dilation limit range. When applying boundary conditions, the bottom, sides, and back of the geometric model are fixed constraints to restrict deformation. The initial stress field is a natural stress field mainly composed of self-weight stress. The initial vertical in situ stress of the model was estimated according to the gravity of the rock mass. The vertical in situ stress increased from the top to the bottom of the model due to gravitational loading. Meanwhile, the automatic joint generator is invoked through command flow to generate tetrahedral finite difference elements to fill the block.

The lithology of the geological model was set as sandstone and slate. The rock thickness was set to 10 m (average rock thickness). This model range of the Z-axis, Y-axis, and X-axis was 0–150 m, 0–270 m, and 0–210 m, respectively.

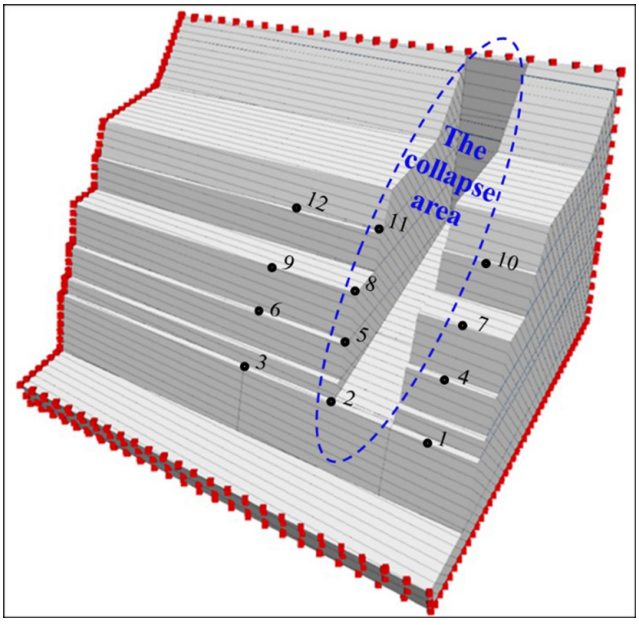

Fig. 10 A simplified model for numerical simulation

The parameters of the rock mass and discontinuities for this numerical simulation are determined on the base of the geomechanical surveys, laboratory rock mass mechanics tests results of the typical toppling rock slope on the right bank of Jiacha hydropower station, literature statistical data and empirical estimations [42], as shown in Table 1.

4.2 Simulation results and analysis

The influence of the numbers of free faces on the displacement was revealed by 3DEC. From the results of the simulation, it is clear that the slope with three free faces has the largest deformation, the displacement contour shown in Fig. 11. From the results presented above, it is well recognized that the numbers of free faces caused by excavation has a significant impact on the stability of slopes. Furthermore, the slope with a free face primarily undergoes a "U" shaped outward bulging deformation in the middle of the free face. In addition, it is also clear that ‚Book-style' bending toppling occurs on the slope with two free faces, its displacement decreased from the slope surface to the inside and from upslope to downslope, and the slipping surface is fan-shaped. At the same time, it can be also observed that the deformation of the slope with three free faces decreased from the slope surface to the inside and the shape of the sliding surface is linear, this will further evolve into a linear fracture and the overall failure will occur. The numerical simulation results presented above reveal that more free faces could increase the probability of slope instability, and thus it should be emphasized that the excavation of multiple free faces should be avoided in the process of engineering construction as much as possible and the preventive engineering measures should be performed on the slope in time.

In order to systematically and deeply study the number of free faces as a key factor affecting the deformation characteristics of toppling rock slope, 12 monitoring points were set up on the model (Fig. 10). The displacement of these monitoring points under different analysis steps and in different directions as illustrated in Fig. 12. And it can be clearly observed that all of the curves in

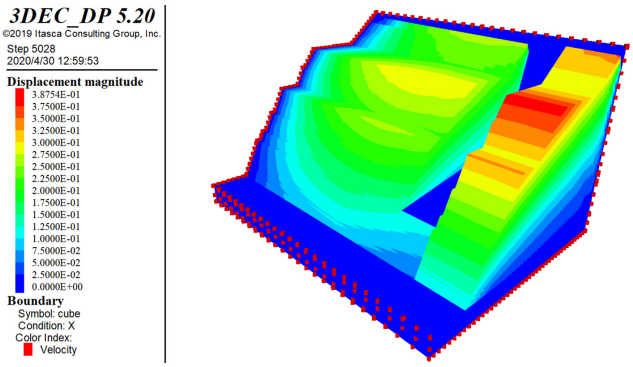

Fig. 11 Displacement cloud map of numerical simulation

the same direction show similar trends. In the left two parts of Fig. 13, the displacements of the two free faces slope in the X and Z-direction firstly increase slowly, rapidly increase after 500 steps, and then tend to be stable at 1700 steps. The deformation gradually decreases from top to bottom, and gradually decreases in the slope from the surface near the open space, which is consistent with the field monitoring data. The displacement generated in the X direction is the largest, and the bending deformation is the most obvious. The typical characteristic of the toppling rock slope is that the deformation in the Y direction is the weakest. This is due to the fact that the rock

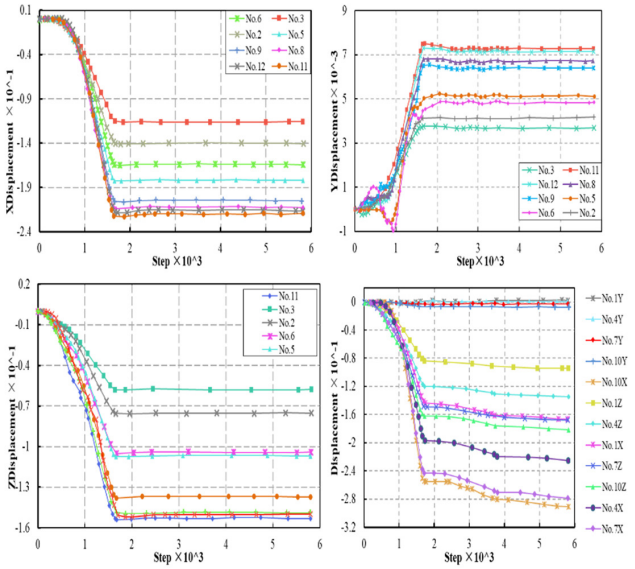

Fig. 12 Monitoring displacement curves of numerical simulation

Table 1 Mechanical Parameter selection table of numerical simulation

Object	Density / kg × m^{-3}	Bulk modulus /GPa	Shear modulus /GPa	Cohesion / MPa	Friction /°	Tensile strength /MPa	Normal stiffness / GPa × m^{-1}	Shear stiffness / GPa × m^{-1}
Rock	26	2.1	1.14	5	45	0.7	-	-
Structural Plane	-	-	-	0.09	30	-	5	6

layer and the side surface are nearly perpendicular, resulting in insignificant deformation in this direction The Y-direction deformation of the three free faces slope is the smallest, the X-direction deformationis obvious, and the displacement in each direction gradually decreases from top to bottom.

Single free face rock mass slope is mainly controlled by the dominate joints set and wedge sliding occurred in this slope (Fig. 13(a): Part 1). Moreover, this slope was also influent by the unloading effect, so the prismatic sliding occurred in the slope toe (Fig. 4). In the double free faces rock mass slope, the combination of the free face and joint set controls the failure model of the toppling rock mass slope [33]. This failure mode can be summarized as unloading and rebounding – dumping and breaking – bulging – shearing – overall failure. In this paper, three dominant joints cut the strata and wedge sliding along the intersection line of two discontinuities occurred [34] (Fig. 13(b): Part 2). However, after the upstream potential collapse area (B area) is affected by the collapse area and forms a three-face void, the rock slope with three free faces could first bend and then slides along a discontinuity under the action of its own weight and unloading (Fig. 13(a): Part 1) [26–27, 41].

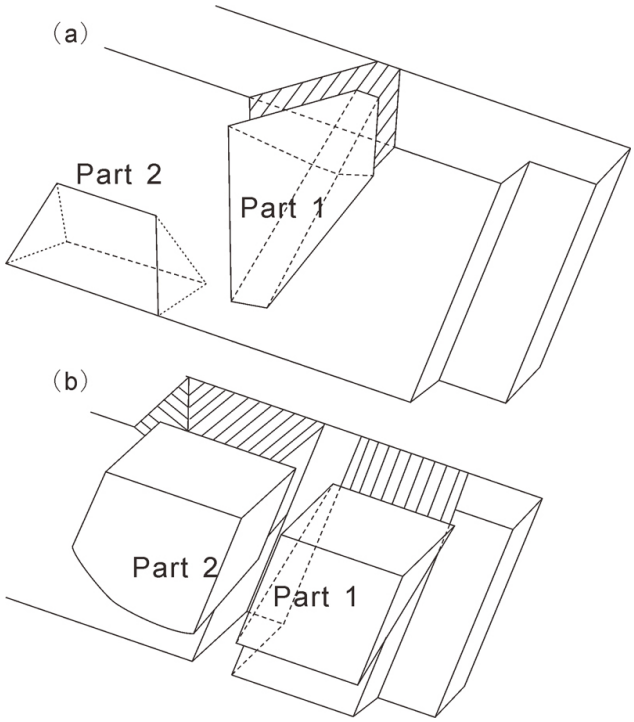

Fig. 13 Sliding and toppling failure model for rock mass slope with (a) one free face; (b) double, and three free faces

5 Disscusion

5.1 Favorable conditions for the formation of the toppling rock slope

The formation conditions for toppling rock slopes have been well recognized by many researchers. However, the development of toppling rock slopes with different numbers of free faces caused by excavation is worthy of study. Both internal and external factors affect toppling events.

The toppling failure mechanism and failure process of the toppling rock slope are complex and it is affected by topography, geological structure, rainfall, earthquakes, gravity, in situ stress and lithology, dip angle and rock thickness [6]. According to the deformation characteristics of the toppling rock slope during the excavation, the triggering factors and causes that lead to the destruction of toppling rock slopes can be divided into five reasons:

1. Geomorphic property: Jiacha Hydropower Station is located in southwest China, there are large areas of metamorphic and sedimentary rock strata, which are influenced by the uplift of the Qinghai-Tibet Plateau. In the western region around the Qinghai-Tibet Plateau, special topographic features with high steep slopes and deep river valleys have been formed, giving birth to numerous high steep toppling rock slopes. Therefore, the topography of the Jiacha bank slope is steep, the slope height is roughly 100 m and the average slope of the slope is approximately 65°, which makes the bank slope in relatively good airside condition. Moreover, the right side of the slope is a gully and the formation of the rock layer is opposite to the landslide, which controls the failure model of the slope. This topography provides conditions for the rock mass movement.
2. Geological properties: Jiacha Hydropower Station is located in Gacha County, Shannan Region, Tibet Autonomous Region, adjacent to the middle section of the main stream of the Yarlung Tsangpo River. The deformation and failure of the toppling soft rock slopes, which are concentrated on the southeastern boundary of the Qinghai-Tibet Plateau, are strongly associated with high horizontal tectonic stresses created by the Cenozoic collision of the India and Eurasia plates [41, 43] and the intensive stress release caused by rapid river incision [44–45]. In addition, the data from the detailed field investigation indicate that the composition of the Jiacha Hydropower Station bank slope of this slope is a thin laminated

rock body within the steeply inclined slope, and the attitude of rocks with the bank slope at a small angle, so this slope is prone to bending and tipping outward. According to the laboratory test and in-situ tests indicate that the slope lithology is mainly composed of thin-layered and medium-thick-layered metamorphic sandstone, siliceous slate and sericite quartz schist, and the saturation compressive strength of these rock groups is in the range of 20–60 MPa. Moreover, the carbonaceous slate developed vertical fractures that provided channels for rainfall infiltration, and it also belongs to the soft rock. At the same time, under the effect of rock-water interactions, the strength of carbonaceous slate decreases obviously. Therefore, under such geological conditions, the rock layer is more prone to bending and dumping deformation.

3. Fault: Several tectonic zones of different sizes randomly developed in the rock body of the slope, which destroyed the integrity of the rock body of the slope. There is a general normal fault that is mainly concentrated on the inner slope of No. 2 highway and near the opening line. In addition, the width of the fault fracture zone and the influence zone is about 1–3 m, which is mainly composed of dense cleavage and quartz vein lenses formed by strong deformation of carbonaceous siliceous slate. Therefore, the base rock on the slope's uphill side has a thick, heavily worn layer with formed fractures. It could be the reason that the uphill had larger deformation than the middle part of the slope. Because of the existence of these faults will result in the drilling process of anchor holes often encountering the phenomenon of stuck drilling, non-return wind and non-return water, and these parts are often affected by the tectonic zone and there are certain geological defects. During excavation, the deformation of rock mass and the uneven redistribution of stresses due to the shearing and movement of tectonic zones, the tectonic zone can become the main path for slope instability and sliding, causing local instability and subsequently leading to slope sliding, slipping, and collapse. Through on-site drilling exploration, we have discovered a tectonic zone intersecting obliquely on the rocky slope, some freely suspended rock blocks will form, and these blocks will gradually approach the surface of the slope, resulting in the formation of free faces. In addition, the tectonic zone may also increase the instability of the rock mass, further exacerbating the deformation and damage of the slope, thereby triggering more free faces.
4. Underground water: Data from the detailed field investigation shows that the factor of safety for slopes can decrease significantly with increasing the groundwater level, and the impact is more significant on slopes with steeper joints. For example, after the rain and snowfall in mid-January 2015, ice and snow melt water infiltrated along the surface cracks, and the infiltration of ice and snow melt water reduced the physical and mechanical strength of the rock body on the one hand, and made the deformation modulus of carbonaceous slate in the rock body of the slope significantly reduced on the other hand, making the slope appear deformation and compression space. In addition, the volume of the groundwater expands after freezing, and the ice-splitting effect is unusually powerful, further increasing the crack opening width. Furthermore, the alternating effect of positive and negative temperatures during day and night, and the repeated freezing and thawing of fracture water, lead to large deformation of the slope. Thus, the slope had obvious deformation where the groundwater outcropped. Fig. 10 shows the outlet locations of groundwater, and this underground water outcropping is mainly located in the collapse area. The water content has a great effect on the compressive strength of the carbonaceous slate which decreases by 48.8% under saturation state and its softening coefficient is 0.52. After excavation, the underground water is developed and outcropped (Fig. 14). Moreover, the downslope was excavated over 50 m, and the unload rebound crack/fracture of rock mass is serious. As a result, the downslope is easy to fail and the deposit is fragmented (Fig. 3). Without the reinforcement of the downslope, the middle portion of the landslide gradually deforms and many tension cracks are formed. The A5 area

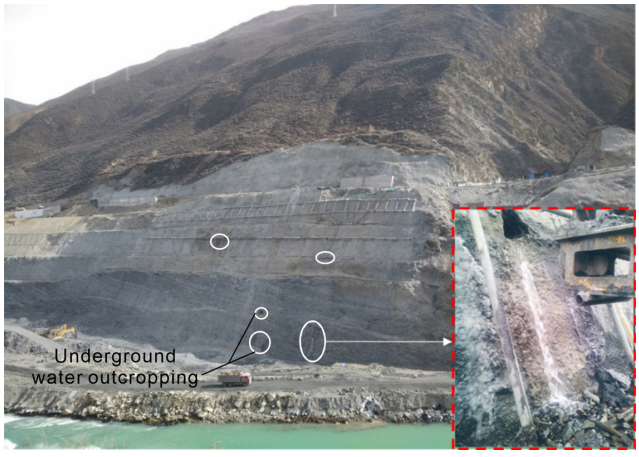

Fig. 14 The outcropping of the spring water

slipped which provides a new free face for the dumping deformation zone. This slope is divided into two parts with two and three free faces, respectively.

5. Engineering: The rock body of the slope itself has the phenomenon of unloading dumping under natural conditions. The excavation of the slope causes the readjustment of the stress, which will produce the tensile stress inclined to the outside of the slope. This will make the originally existing unloading cracks further outward tension, which will have adverse effects on the stability of the slope, and then lead to the deformation of the slope. Moreover, the deformation of the slope accelerated after a blasting, because the influence of blast dynamic load on the stresses of the rock slope is significant, and the maximum principal stress is concentrated at the toe of the slope. The blast dynamic load also leads to more fragmentation of the rock mass.

In conclusion, under the integrative action of the fault, unloading, gravity, in situ stress and groundwater, the toppling rock slope's upward progressively bending and deforming. The bending rock layer pushes and compresses the middle and front parts of the slope. The dynamic load is the main factor causing the failure of the slope. In the initial stage of excavation, the rate of dumping deformation increased, the horizontal displacement led to the protrusion of the slope, the vertical downward displacement increased rapidly, and the uphill part of the slope was deformed and affected to a greater depth. In the late stage of excavation, the deformation of the rock slope decreases and the slope gradually self-stabilizes. At the same time, under the softening of groundwater and compression of rock mass, the middle and uphill parts of the A5 area slipped and is cut out from the first berm path, while the lower rock mass is compressed and broken, and local collapse occurred (Fig. 15). The upper part of the slope produces many local collapses.

5.2 Failure mechanism of the toppling rock slope with different numbers of free faces

A single free-face slope, constrained by both sides and the base, primarily undergoes deformation controlled by joints. Under the influence of gravity and unloading, deformation tends to concentrate in the middle of the free face, presenting a bulging phenomenon in the center. Typically, the deformation is minor, resulting in 'wedge-shaped body' failure (Fig. 13(a)), and primarily develops disasters such as collapses. After such slopes are predisposed to disaster, the continuous fracturing and collapsing of the rock mass provide a free face for the remaining rock body.

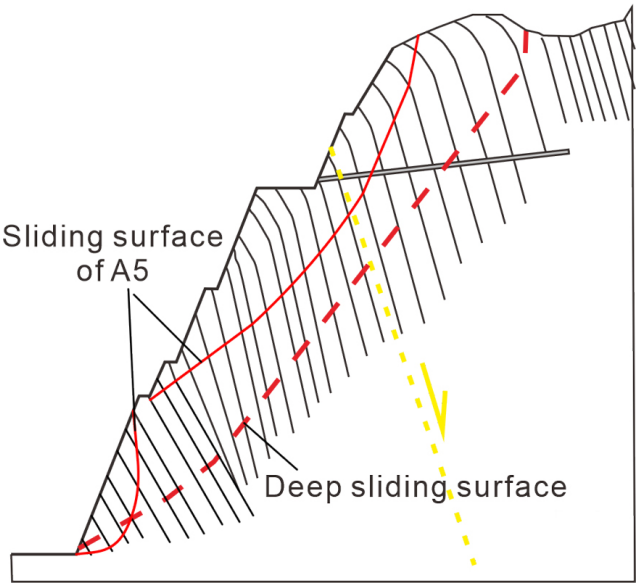

Fig. 15 Failure model of the Jiacha slope

Two free faces define slopes with one side and the front edge, which are frequently created by river or valley cutting or impacted by human engineering activity. These slopes are controlled by reverse-dipping structural planes. Under the effects of unloading and gravity, stress concentration occurs at the junction of the free faces, leading to 'book dumping' deformation. The front face of the slope undergoes outward tilting deformation due to gravity and unloading. The lateral free face experiences tensile forces under unloading and gravity, causing micro-cracks formed by tectonic actions to gradually extend and form through-going vertical cracks. When the locked segment of the rock mass lacks sufficient tensile strength to resist external forces, the rock layer fails, and the cross-section of the rock layer appears arc-shaped. Due to stress concentration, deformation mainly concentrates at the intersection of the two free faces, presenting a fan-shaped distribution. Due to the rock strata's orientation being nearly parallel to the slope's direction, under the influence of gravity, the slope body tends to move towards the free face at the front, resulting in the formation of tensile cracks at the slope crest that align with the strata's orientation. Concurrently, because of the lateral free face, the slope body exhibits a tendency to move towards the lateral free face under the influence of gravity. When the tensile strength of the rock mass is less than the combined external forces, the slope gradually evolves and forms overall failure, leading to disasters such as collapses and landslides.

The slope is unconstrained on three sides and controlled by joints under external forces, causing the rock layers to bend and topple towards the front, forming a typical 'nodding' bending and toppling deformation failure mode. Rainwater infiltrates from the rock layer surfaces into the interior of

the slope, soaking and softening the interlayer cementation, which weakens the interconnection between rock masses and accelerates the transfer of material, reducing the strength of the rock body. This typical reverse-dipping rock slope, due to the release of constraints on both sides, is equivalent to the two-dimensional case commonly studied and conforms to the cantilever beam model, with tension on the backside and compression at the bottom. Based on the cantilever beam bending model and using the limit equilibrium theory, when the tensile stress of the rock layer exceeds its tensile strength, toppling instability failure occurs, and the slope forms a through-going failure surface, primarily characterized by large-scale and overall failure.

6 Conclusions

In this study, a deformation and failure model of a toppling rock slope in the Jiacha Hydropower Station area in Southwest China is proposed under multiple numbers of free faces. The failure mode and deformation evolution process of the toppling rock slope under different numbers of free faces caused by excavation are studied by combining on-site investigation, deformation monitoring and numerical simulation. Several conclusions can be drawn:

1. In the study area, the slope firstly was excavated over 50 m and formed an unloaded zone. The rock structure is broken under the action of gravity and faults. The developed underground water increases the water content of rock and decreases the strength of the carbonaceous slate. Therefore, wedge sliding occurred. The shallow rock layer gradually deformed and local collapse occurred and many cracks were found in the slope surface. There is a prismatic sliding at the toe of the slope due to the unloaded zone effect.
2. After excavating to the wedge sliding, the slope was divided into two parts with double and three free faces, respectively. The deformation and failure modes, deformation characteristics and formation mechanisms of toppling rock slopes with different numbers of free faces are different. Under the condition of a free face, the toppling rock slope is dominated by collapse, collapse, slip and other modes, usually with small-scale deformation; Under the condition of two free faces, the slope is mainly deformed by 'book dumping', the section of rock stratum is in the shape of arc-shaped, and a fan-shaped deformation area is formed at the intersection of the two free faces, which can breed disasters such as collapse and landslide; Under the condition of three free faces, the slope forms a typical bending and dumping deformation failure mode of 'nodding and slouching type', and the penetration failure surface is dominated by the overall failure.
3. Based on the results of field monitoring and numerical simulation, it can be seen that the free face amount has an important effect on the deformation characteristics and failure model of the rock slope. The deformation of the slope with one free face mainly occurred in the middle section. Three dominant joints cut the strata and wedge sliding along the intersection line of two discontinuities that occurred in the double free faces rock slope. However, in the three free faces rock slope, a sliding zone was formed along the discontinuity, and the rock sliding mass slid.

7 Acknowledgment

The author sincerely acknowledges the supported by Open Project Funding of Key Laboratory of Intelligent Health Perception and Ecological Restoration of Rivers and Lakes, Ministry of Education, Hubei University of Technology; Under the erosion effect of river water scouring, the anti-erosion mechanism of a new type of ecological brick protective bank slope (HGKFZP004); The Joint Funds of the National Nature Science Foundation of China (No. U22A20232); The Fundamental Research Funds for the Central Universities (No. 2022CFB833, No. Q20275408, No. 2021QN1082, No. XJ2021000502); The Regional Key Research and Development Program of Xinjiang Province (No. 2021B03004-3); Ph.D. research start-up fund of Hubei University of Technology, China: Study on the evolution law of THMC characteristic parameters and constitutive model of solidified marine clay (No. XJ2021000502); Natural Science Foundation of Hubei Province, China: Spatial-temporal dynamic evolution mechanism of soil moisture in ecological protection slopes under rainfall conditions (No. 2022CFB833); Young and middle-aged talent project of the Science and Technology Research Program of the Hubei Provincial Department of Education, China: Experimental study on the mechanism of buried anti-slide piles and plants synergistic slope protection under rainfall conditions (No. Q20275408); Anti-erosion mechanism of new ecological brick revetment slope under the action of river water erosion (No. HGKFZPO03); The open Project Funding of Key Laboratory of Intelligent Health Perception and Ecological Restoration of Rivers and Lakes, Ministry of Education, Hubei University of Technology (No. HGKFZPO03); Shanxi Province Transportation Technology Research and Development CO.,LTD.

References

[1] Chen, Z. Y., Gong, W. J., Ma, G. W., He, L., Xing, Y. C., Xing, J. Y. "Comparisons between the centrifuge and numerical modeling results for slope toppling failure", Science China Technological Sciences, 58(9), pp. 1497–1508, 2015. https://doi.org/10.1007/s11431-015-5889-x

[2] Xie, L., Yan, E., Ren, X., Lu, G. "Sensitivity analysis of bending and toppling deformation for anti-slope based on the grey relation method", Geotechnical and Geological Engineering, 33, pp. 35–41, 2015. https://doi.org/10.1007/s10706-014-9817-9

[3] Li, Z., Wang, J., Li, L., Wang, L., Liang, R. Y., "A case study integrating numerical simulation and GB-InSAR monitoring to analyze flexural toppling of an anti-dip slope in Fushun open pit", Engineering Geology, 197, pp. 20–32, 2015. https://doi.org/10.1016/j.enggeo.2015.08.012

[4] Li, L.-Q., Ju, N.-P., Zhang, S., Deng, X.-X., Sheng, D. "Seismic wave propagation characteristic and its effects on the failure of steep jointed anti-dip rock slope", Landslides, 16, pp. 105–123, 2019. https://doi.org/10.1007/s10346-018-1071-4

[5] Azarafza, M., Akgün, H., Ghazifard, A., Asghari-Kaljahi, E. "Key-block based analytical stability method for discontinuous rock slope subjected to toppling failure", Computers and Geotechnics, 124, 103620, 2020. https://doi.org/10.1016/j.compgeo.2020.103620

[6] Li, X. B., Dong, L. J., Zhao, G. Y., Huang, M., Liu, A. H., Zeng, L. F., Dong, L., Chen, G. H. "Stability analysis and comprehensive treatment methods of landslides under complex mining environment – a case study of Dahu landslide from Linbao Henan in China", Safety Science, 50(4), pp. 695–704, 2012. https://doi.org/10.1016/j.ssci.2011.08.049

[7] Tao, Z., Geng, Q., Zhu, C., He, M., Cai, H., Pang, S., Meng, X. "The mechanical mechanisms of large-scale toppling failure for counter-inclined rock slopes", Journal of Geophysics and Engineering, 16(3), pp. 541–558, 2019. https://doi.org/10.1093/jge/gxz020

[8] Tiedeu, W. N., Jiang, D., Chen, J., Fan, J. "A review on rock slope stability: failure mechanisms, stabilization techniques and implications for mining engineering", Geotechnical Engineering, 51(4), 00465828, 2020.

[9] Zhu, C., He, M., Karakus, M., Cui, X., Tao, Z. "Investigating toppling failure mechanism of anti-dip layered slope due to excavation by physical modelling", Rock Mechanics and Rock Engineering, 53, pp. 5029–5050, 2020. https://doi.org/10.1007/s00603-020-02207-y

[10] Chen, M.-L., Lv, P.-F., Nie, W.-Z., Tan, C.-M., Bai, Z.-H., Liao, Y., Zhou, J.-W. "The role of water and lithology on the deformation and failure of an anaclinal rock slope in a hydropower reservoir", Advances in Civil Engineering, 2020(1), pp. 1–13, 2020. https://doi.org/10.1155/2020/8852227

[11] Tan, R. J., Yang, X. Z., Hu, R. L. "Review of deformation mechanism and stability analysis of anti-dipped rock slopes", Rock and Soil Mechanics, 30(Z2), pp. 479–484, 2009. https://doi.org/10.16285/j.rsm.2009.s2.087

[12] Zhu, C., Huang, Y., Sun, J. "Solid-like and liquid-like granular flows on inclined surfaces under vibration–Implications for earthquake-induced landslides", Computers and Geotechnics, 123, 103598, 2020. https://doi.org/10.1016/j.compgeo.2020.103598

[13] Yang, J., Liu, J., Qin, Z., Tang, X., Zhang, H. "Multiscale modeling of gas-induced fracturing in anisotropic clayey rocks", Journal of Rock Mechanics and Geotechnical Engineering, 16(6), pp. 2091–2110, 2024. https://doi.org/10.1016/j.jrmge.2024.03.011

[14] Zhang, C., Jin, Z., Feng, G., Song, X., Rui, G., Yujiang, Z. "Double peaked stress-strain behavior and progressive failure mechanism of encased coal pillars under uniaxial compression", Rock Mechanics and Rock Engineering, 53(3), pp. 3253–3266, 2020. https://doi.org/10.1007/s00603-020-02101-7

[15] Han, B. C., Wang, S. J. "Mechanism for toppling deformation of slope and analysis of influencing factors on it", Journal of Engineering Geology, 7(3), pp. 213–217, 1999.

[16] Cheng, D.-X., Liu, D.-A., Ding, E.-B., Zhao, H.-M., Pan, W., Guo, H.-F."Analysis on influential factors and toppling conditions of toppling rock slope", Chinese Journal of Geotechnical Engineering, 27(11), pp. 1362–1366, 2005.

[17] Amini, M., Majdi, A., Aydan Ö. "Stability analysis and the stabilization of flexural toppling failure", Rock Mechanics and Rock Engineering, 42(5), pp. 751–782, 2009. https://doi.org/10.1007/s00603-008-0020-2

[18] Majdi, A., Amini, M. "Analysis of geo-structural defects in flexural toppling failure", International Journal of Rock Mechanics and Mining Sciences, 48(2), pp. 175–186, 2011. https://doi.org/10.1016/j.ijrmms.2010.11.007

[19] Huang, R., Li, Y., Yan, M. "The implication and evaluation of toppling failure in engineering geology practice", Journal of Engineering Geology, 25(5), pp. 1165–1181, 2017. https://doi.org/10.13544/j.cnki.jeg.2017.05.001

[20] Gu, D. M., Gao, X. C., Zhang, W. G., Da, H., Xun, W. "Failure evolution of anti-dip rock slope in the three Gorges reservoir area", Rock and Soil Mechanics, 41(Z2), pp. 1–10, 2020. https://doi.org/10.16285/j.rsm.2020.0394

[21] Müller L. "The rock slide in the Vajont valley", Rock Mechanics Engineering Geology, 2, 2(3), pp. 148–212, 1964.

[22] Goodman, R. E., Bray, J. W. "Toppling of rock slope, ASCE. Speciality Conference", Rock Engineering for Foundation and Slopes, 2, pp. 201–234, 1976.

[23] Anderson, M. G., Richards, K. S. "Slope stability", John Wiley and Sons, pp. 187–230, 1987.

[24] Zhang, Z., Whang, S., Wang, L. "Principles of Engineering Geological Analysis", Geological Publishing House, Beijing, 2009.

[25] Liu, C. H., Jaksa, M. B., Meyers, A. G. "Improved analytical solution for toppling stability analysis of rock slopes", International Journal of Rock Mechanics and Mining Sciences, 45(8), pp. 1361–1372, 2008. https://doi.org/10.1016/j.ijrmms.2008.01.009

[26] Bobet, A. "Analytical solutions for toppling failure", International Journal of Rock Mechanics and Mining Sciences, 36(7), pp. 971–980, 1999. https://doi.org/10.1016/S0148-9062(99)00059-5

[27] Yokoyama O. "Evolution of uphill-facing scarps by flexural toppling of slate with high-angle faults", Geomorphology, 352, 106977, 2020. https://doi.org/10.1016/j.geomorph.2019.106977

[28] Yi, X. J., Yan, E. C., Sun, Z. L. "Slip surface ascertaining and stability analyzing of the countertendency shale slope", Rock and Soil Mechanics, 2007, 28(Z1), pp. 595–598. https://doi.org/10.16285/j.rsm.2007.s1.137

[29] Amini, M., Golamzadeh, M., Khosravi, M. "Physical and theoretical modeling of rock slopes against block-flexure toppling failure", International Journal of Mining and Geo-Engineering, 49(2), pp. 155–171, 2015. https://doi.org/10.22059/IJMGE.2015.56103

[30] Amini, M., Sarfaraz, H., Esmaeili, K. "Stability analysis of slopes with a potential of slide-head-toppling failure", International Journal of Rock Mechanics and Mining Sciences, 112, pp. 108–121, 2018. https://doi.org/10.1016/j.ijrmms.2018.09.008

[31] Bowa, V. M., Xia, Y. "Influence of counter-tilted failure surface angle on the stability of rock slopes subjected to block toppling failure mechanisms", Bulletin of Engineering Geology and the Environment, 78(4), pp. 2535–2550, 2018. https://doi.org/10.1007/s10064-018-1253-2

[32] Zheng, D., Wang, Q., Mao, F. "Centrifuge model test study on the key hazard factor of deep toppling deformation and disaster pattern of counter-tilt layered rock slope", Chinese Journal of Rock Mechanics and Engineering, 38(10), pp. 1954–1963, 2019. https://doi.org/10.13722/j.cnki.jrme.2018.1484

[33] Yoon, W. S., Jeong, U. J., Kim, J. H. "Kinematic analysis for sliding failure of multi-faced rock slopes", Engineering Geology, 67(1/2), pp. 51–61, 2002. https://doi.org/10.1016/S0013-7952(02)00144-8

[34] Wang, L. Q., Tang, H. M., Liang, Y., Wu, X. "Kinematic analyses of sliding and toppling failure of double free face rock mass slopes", Rock and Soil Mechanics, 32(Z1), pp. 72–77, 2011. https://doi.org/10.16285/j.rsm.2011.s1.010

[35] Nichol, S. L., Hungr, O., Evans, S. G. "Large-scale brittle and ductile toppling of rock slopes", Canadian Geotechnical Journal, 39(4), pp. 773–788, 2002. https://doi.org/10.1139/t02-027

[36] Zhang, Z., Wang, T., Wu, S., Tang, H. "Rock toppling failure mode influenced by local response to earthquakes", Bulletin of Engineering Geology and the Environment, 75, pp. 1361–1375, 2016. https://doi.org/10.1007/s10064-015-0806-x

[37] Cui, Z., Chen, P.-Z., Chu, W.-J., Zhou, Y., Liu, N., Sheng, Q. "Deformation mechanism and reinforcement design for the flexural toppled slope of Miaowei HPP", Bulletin of Engineering Geology and the Environment, 82(1), 39, 2023. https://doi.org/10.1007/s10064-023-03065-y

[38] Braathen, A., Blikra, L. H., Berg, S. S., Karlsen, F. "Rock-slope failures in Norway; type, geometry, deformation mechanisms and stability", Norwegian Journal of Geology/Norsk Geologisk Forening, 84(1), pp. 67–88, 2004.

[39] Ambrosi, C., Crosta, G. B. "Valley shape influence on deformation mechanisms of rock slopes", Geological Society, Special Publications, 351(1), pp. 215–233, 2011. https://doi.org/10.1144/SP351.12

[40] Cai, J.-C., Ju, N.-P., Huang, R.-Q., Zheng, D., Zhao, W.-H., Li, L.-Q., Huang, J. "Mechanism of toppling and deformation in hard rock slope: a case of bank slope of Hydropower Station, Qinghai Province, China", Journal of Mountain Science, 16(4), pp. 924–934, 2019. https://doi.org/10.1007/s11629-018-5096-x

[41] Huang, R. Q., Wang, Y. S., Wang, S. T., Li, Y.-S. "High geo-stress distribution and high geo-stress concentration area models for eastern margin of Qinghai-Tibet plateau", Science China Technological Sciences, 54(1), pp. 154–166, 2011. https://doi.org/10.1007/s11431-011-4652-1

[42] Yao, Y., Zhang, G. C., Chen, H. J., Wang, M. F., Bao, L. L., Chang, Z. "Study on the Failure mechanism of rock slope with layered cataclastic structure", Chinese Journal of Rock Mechanics and Engineering, 40, pp. 365–381, 2021. https://doi.org/10.13722/j.cnki.jrme.2020.0631

[43] Ye, S., Li, Y. S., Guo, Q. "Mechanics research on rock stress and deformation of Lancang river canyon's large-scale dumping deformation", Applied Mechanics and Materials, Trans Tech Publications Ltd, 353, pp. 318–323, 2013. https://doi.org/10.4028/www.scientific.net/amm.353-356.318

[44] Clark, M. K., Royden, L. H., Whipple, K. X., Burchfiel, B. C., Zhang, X., Tang, W. "Use of a regional, relict landscape to measure vertical deformation of the eastern Tibetan Plateau", Journal of Geophysical Research: Earth Surface, 111(F3), 2006. https://doi.org/10.1029/2005JF000294

[45] Hou, Y. L., Chigira, M., Tsou, C.-Y. "Numerical study on deep-seated gravitational slope deformation in a shale-dominated dip slope due to river incision", Engineering Geology, 179, pp. 59–75, 2014. https://doi.org/10.1016/j.enggeo.2014.06.020